Supporting Information

Active Phase on $SrCo_{1-x}Fe_xO_{3-\delta}$ ($0 \leq x \leq 0.5$) Perovskite for Water Oxidation: Reconstructed Surface versus Remaining Bulk

Haiyan Li,[†,#] Yubo Chen,[†,§,#] Jingjie Ge,[†] Xianhu Liu,[Δ] Adrian C. Fisher,[‡,§] Matthew P. Sherburne,[□,ǂ] Joel W. Ager III,[□,ǂ] Zhichuan J. Xu[†,§,ǁ,]*

[†]School of Materials Science and Engineering, Nanyang Technological University, Singapore 639798, Singapore

[§]The Cambridge Centre for Advanced Research and Education in Singapore, 1 CREATE Way, Singapore 138602, Singapore

[‡]Department of Chemical Engineering, University of Cambridge, Cambridge, CB2 3RA, UK

[Δ]Key Laboratory of Advanced Material Processing & Mold (Zhengzhou University), Ministry of Education, Zhengzhou, 450002, China

Department of Materials Science and Engineering, University of California at Berkeley, Berkeley, California 94720, USA

[ǂ]Berkeley Educational Alliance for Research in Singapore Ltd., 1 CREATE Way, Singapore 138602, Singapore

[ǁ]Energy Research Institute@NTU, ERI@N, Interdisciplinary Graduate School, Nanyang Technological University, Singapore 639798, Singapore

Corresponding Author

*E-mail: xuzc@ntu.edu.sg

Author Contributions

[#]These authors contributed equally to this work.

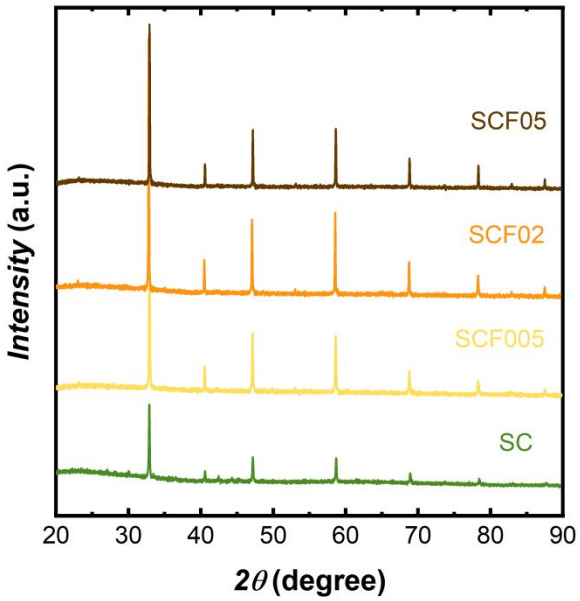

Figure S1. XRD patterns of as-synthesized $SrCo_{1-x}Fe_xO_{3-\delta}$ (x = 0, 0.05, 0.2 and 0.5, denoted as SC, SCF005, SCF02 and SCF05, respectively).

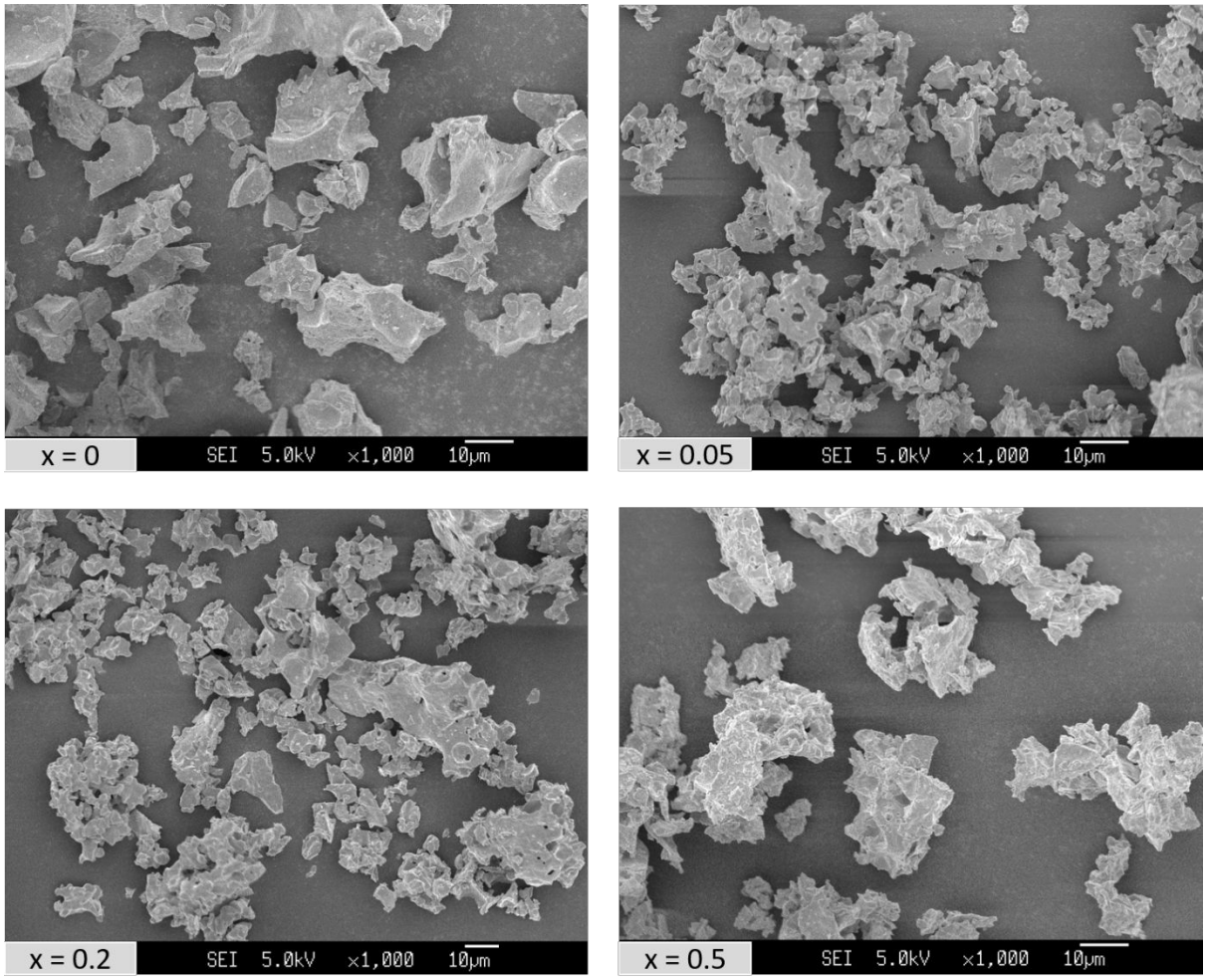

Figure S2. SEM images of as-synthesized $SrCo_{1-x}Fe_xO_{3-\delta}$ (x = 0, 0.05, 0.2 and 0.5).

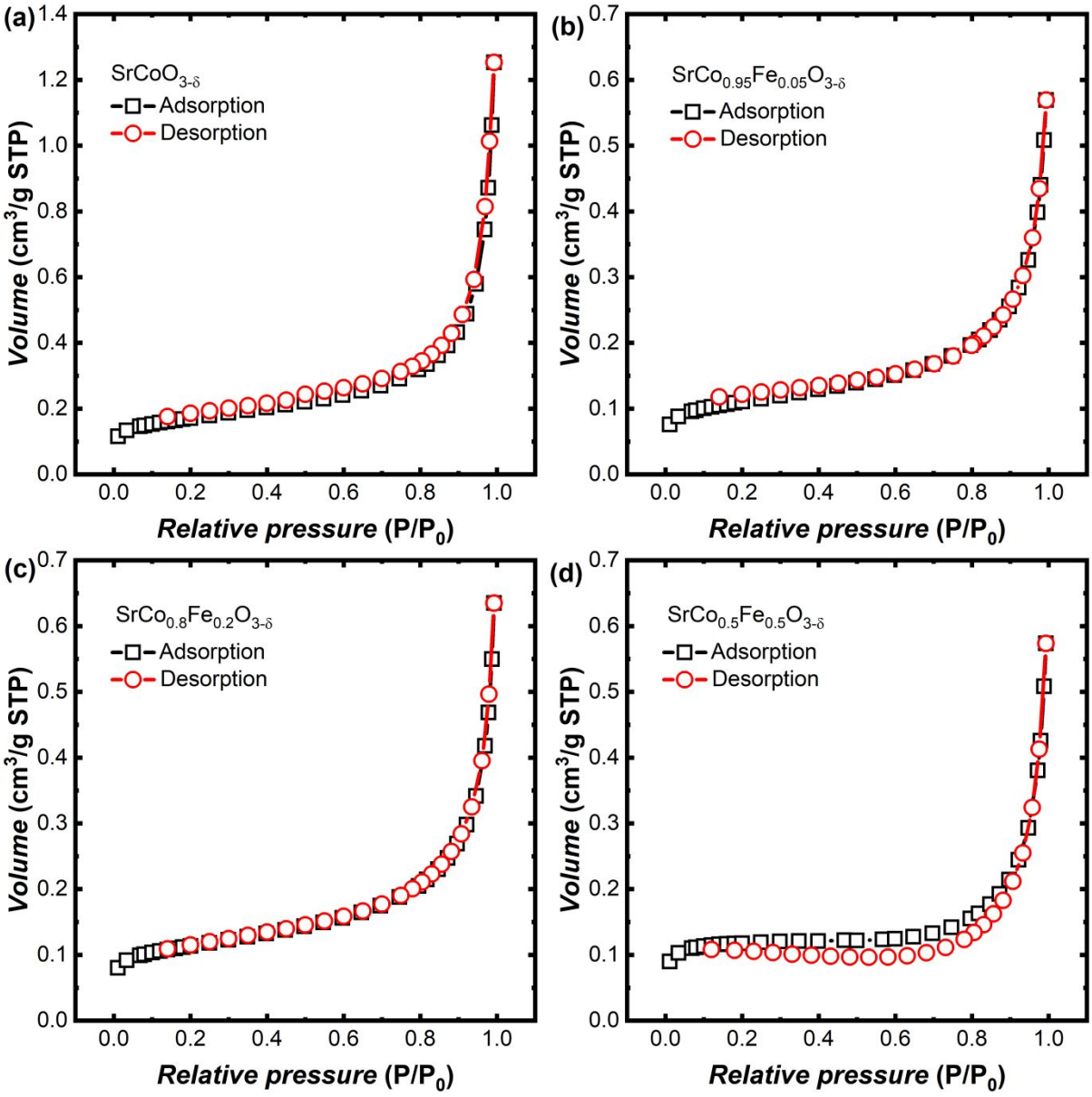

Figure S3. BET measurements of **(a)** $SrCoO_{3-\delta}$, **(b)** $SrCo_{0.95}Fe_{0.05}O_{3-\delta}$, **(c)** $SrCo_{0.8}Fe_{0.2}O_{3-\delta}$ and **(d)** $SrCo_{0.5}Fe_{0.5}O_{3-\delta}$.

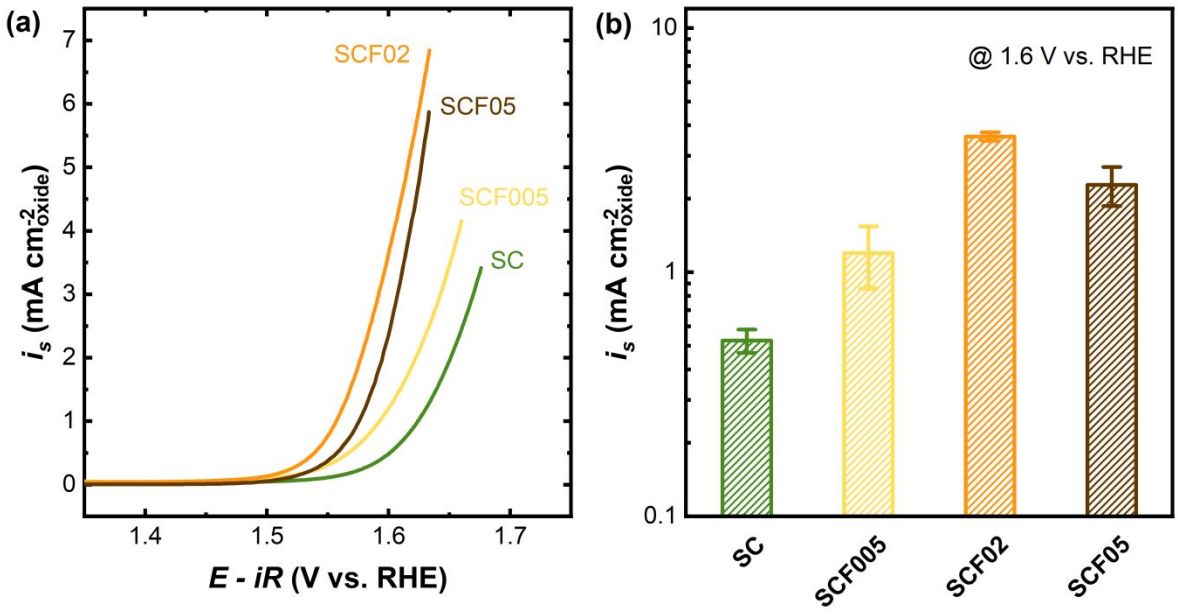

Figure S4. (a) Capacitance- and *iR*-corrected OER currents normalized to the oxide surface area determined by BET measurements for $SrCo_{1-x}Fe_xO_{3-\delta}$ (x = 0, 0.05, 0.2 and 0.5). The electrochemical data were taken from the 100th CV scans in 0.1 M KOH electrolyte. (b) OER specific activities at 1.6 V vs. RHE of $SrCo_{1-x}Fe_xO_{3-\delta}$. Error bars represent standard deviations from three independent measurements.

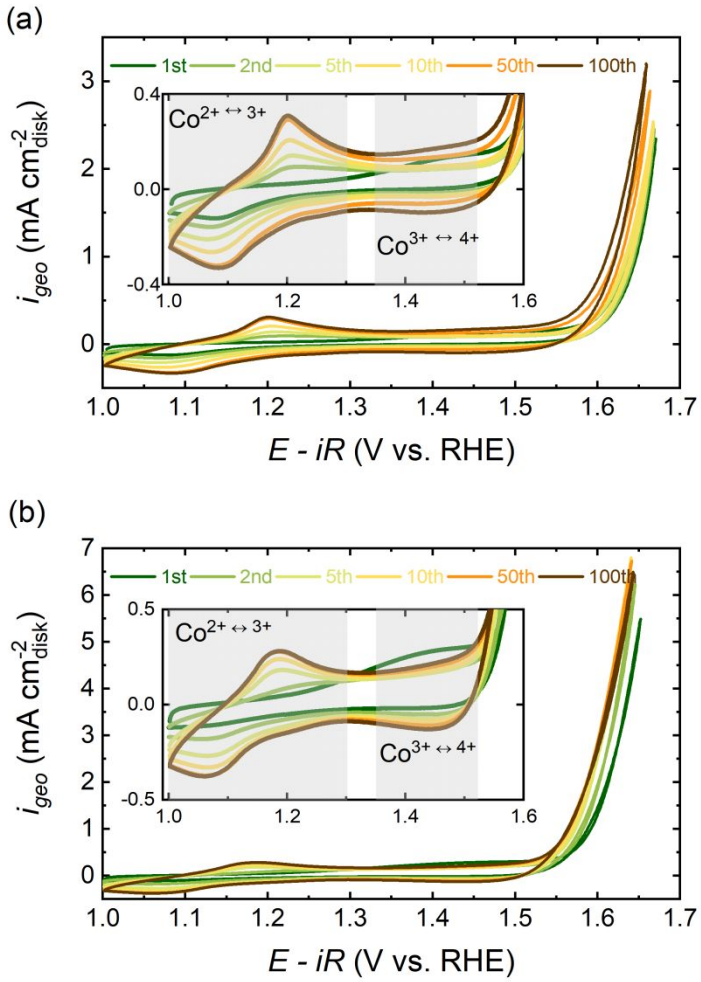

Figure S5. Cyclic voltammograms of (a) SC and (b) SCF02 at a scan rate of 10 mVs^{-1} in 0.1 M Fe-free KOH, showing the 1st, 2nd, 5th, 10th, 50th, and 100th cycles. Insets show the capacitive region of CV scans and the shaded areas indicate the redox waves.

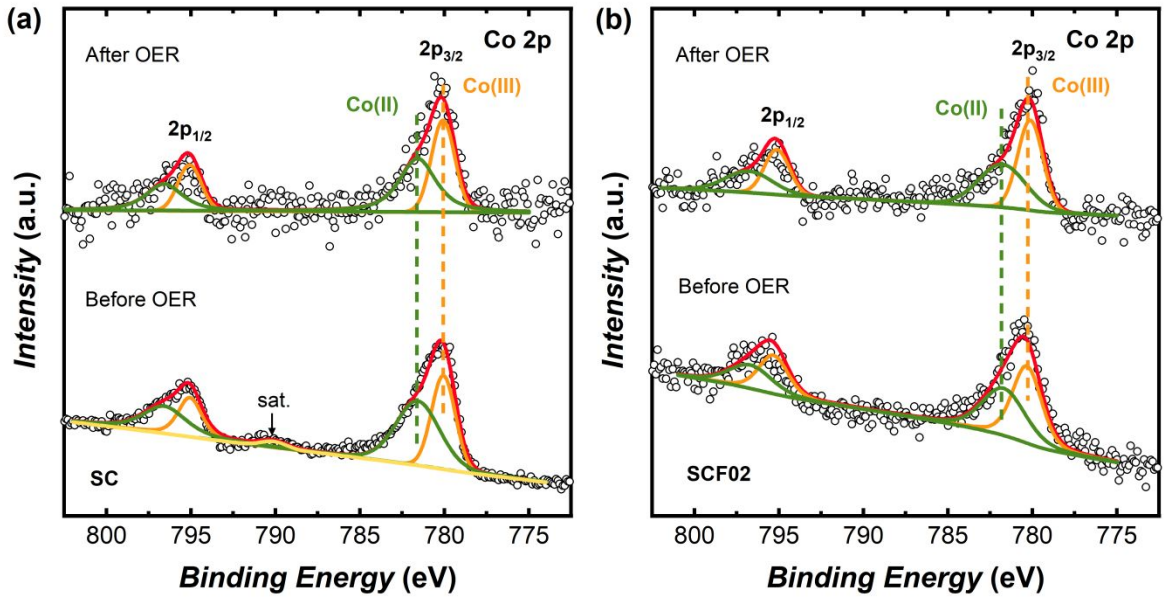

Figure S6. Co 2p XPS spectra of (a) SC and (b) SCF02 before and after OER tests. Insignificant variation in the cobalt oxidation sate was observed for SC as well as SCF02 before and after OER measurements.

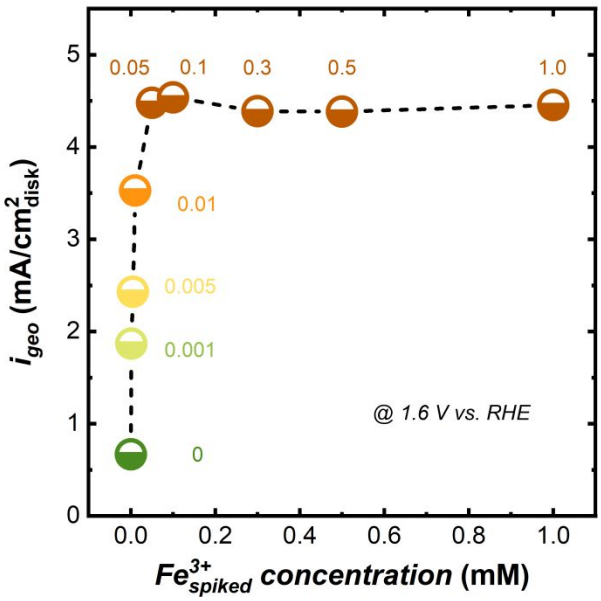

Figure S7. The variation of the geometric current density at 1.6 V vs. RHE with the concentration of Fe^{3+} spiked into the 0.1 M KOH electrolyte.

We note that the optimized Fe^{3+}_{spiked} concentration is ~0.1 mM, which is much higher than the critical value (ca. 10^{-6} M) required for the alkaline electrolyte being saturated with soluble Fe species.[1] A similar result has been reported for amorphous CoO_x + Fe^{3+} catalyst (where the optimized Fe^{3+}_{spiked} concentration is 0.3 mM).[2] Over a CoO_xH_y host, the dissolution of Fe from the electrode and the deposition of Fe from the electrolyte during OER are concomitant.[3] Hence, to ensure sufficiently high content of Fe being incorporated into the reconstructed surface, the deposition rate of Fe, which is positively correlated with the Fe content in the electrolyte, should be equal to or much higher than the dissolution rate.[3] Then, the concentration of Fe^{3+}_{spiked} beyond the solubility limit is expected to make sure that the electrolyte immediately adjacent to the catalyst's surface is always saturated with soluble Fe species. And thus, a sufficient amount of Fe can be maintained in the reconstructed surface of SC, which yields the highest catalytic activity.

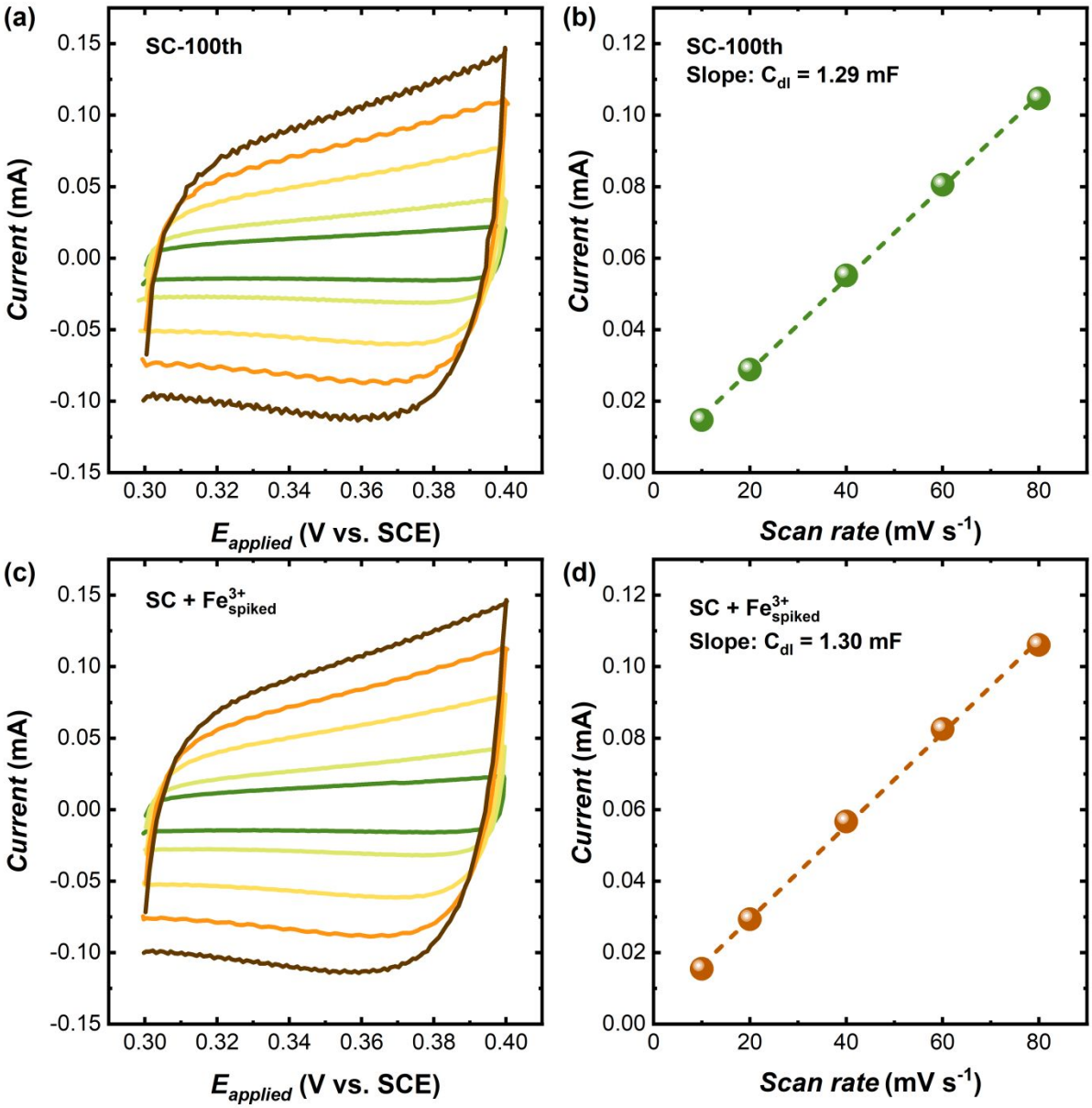

Figure S8. Double-layer capacitance (C_{dl}) measurements for SC in 0.1 M KOH and 0.1 M KOH + 0.1 mM Fe^{3+}_{spiked} electrolytes. Cyclic voltammograms measured at scan rates of 10, 20, 40, 60 and 80 mV/s of (a) SC and (c) SC + Fe^{3+}_{spiked}. The average of the cathodic and anodic charging currents measured at 0.35 V vs. SCE plotted as a function of scan rate for (b) SC and (d) SC + Fe^{3+}_{spiked}. The double-layer capacitances are equal to the slopes obtained from the linear fitting of the two sets of data.

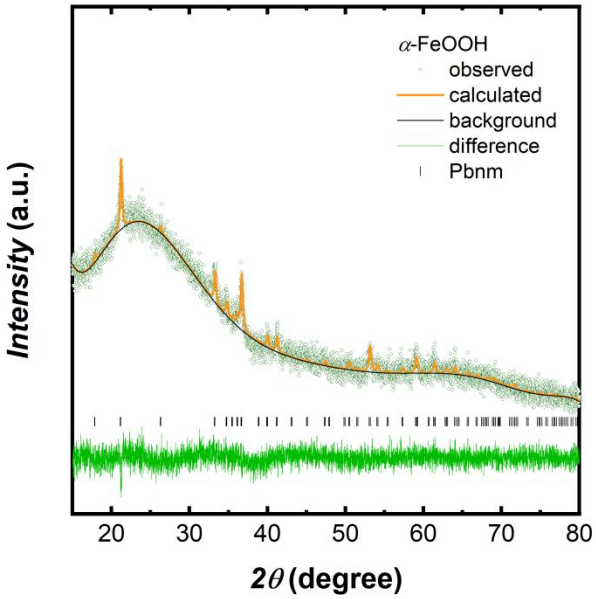

Figure S9. Rietveld refined XRD pattern of α-FeOOH collected from the brown precipitate after adding $Fe(NO_3)_3$ into 0.1 M KOH solution. The reliability factors are R_p = 1.92%, R_{wp} = 2.43%, and χ^2 = 1.11. To collect the precipitate, the KOH electrolyte mixed with aqueous $Fe(NO_3)_3$ solution was shaken and centrifuged, and the supernatant was decanted. Then, the obtained precipitate was dried in air at room temperature.

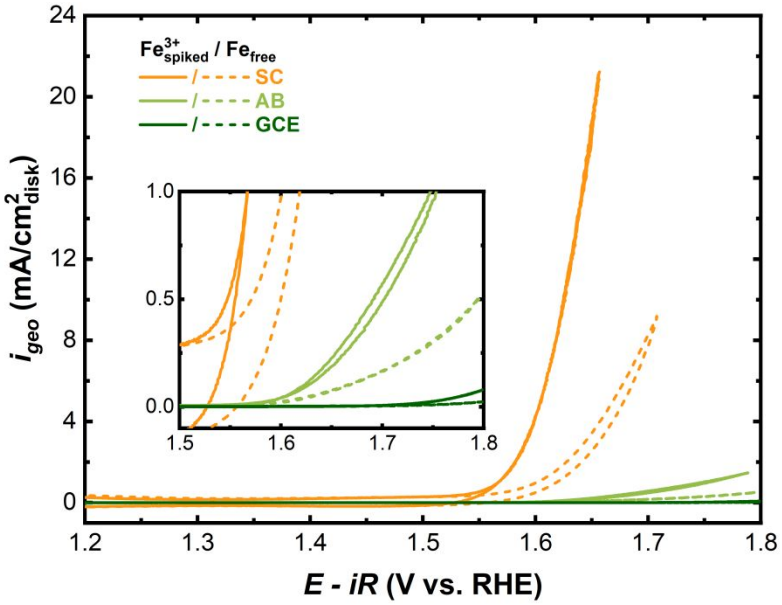

Figure S10. Cyclic voltammograms (10 mVs^{-1}) of SC oxide catalyst (containing 50 µg SC oxide and 20 µg carbon additive (acetylene black, AB)), pure carbon catalyst (containing 20 µg AB) and blank glassy carbon electrode (GCE) in 0.1 M KOH (dashed lines) and 0.1 M KOH + 0.1 mM Fe^{3+}_{spiked} (solid lines).

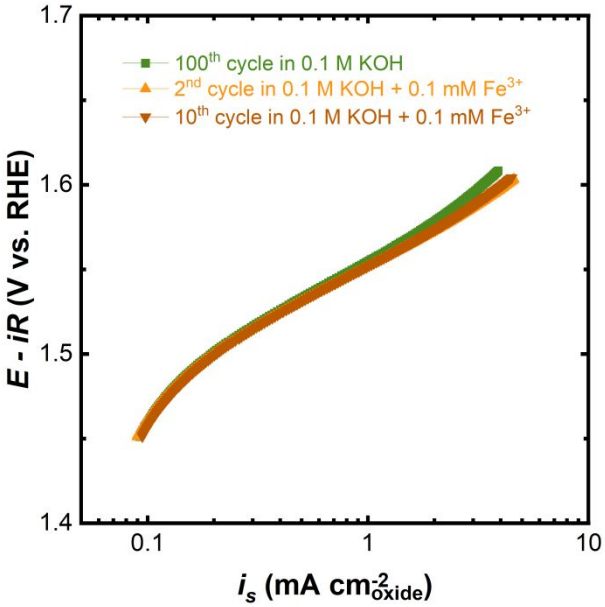

Figure S11. Tafel plots normalized to the oxide surface area for SCF02 in 0.1 M KOH (100^{th} cycle) and 0.1 M KOH + 0.1 mM Fe^{3+}_{spiked} (2^{nd} and 10^{th} cycles). Before cycling in Fe-spiked KOH electrolyte, SCF02 underwent 100 CV scans in Fe-free KOH solution to stabilize its electrochemical behaviour.

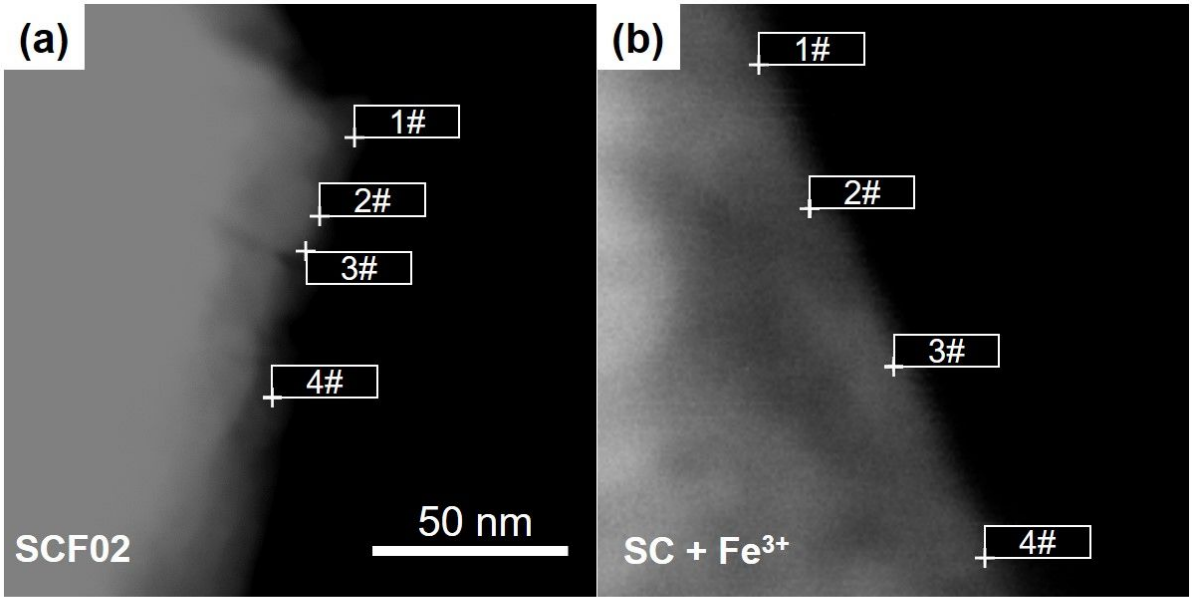

(c)

	SCF02			SC + Fe^{3+}		
	Sr	Co	Fe	Sr	Co	Fe
1#	10.9%	72.8%	16.3%	3.3%	83.3%	13.4%
2#	19.7%	62.5%	17.8%	1.9%	80.2%	17.9%
3#	22.9%	61.4%	15.7%	0.2%	79.4%	20.4%
4#	24.7%	61.0%	14.3%	1.1%	87.5%	11.3%
	Co : Fe ratio = 4.0±0.4			Co : Fe ratio = 5.6±1.5		

Figure S12. High angle annular dark field (HADDF) of (a) cycled SCF02 and (b) cycled SC + Fe^{3+} with point scanning transmission electron microscopy (STEM) energy dispersive X-ray spectroscopy (EDS) analysis. Surface Sr, Co and Fe metal ratios determined by STEM EDS are summarized in (c).

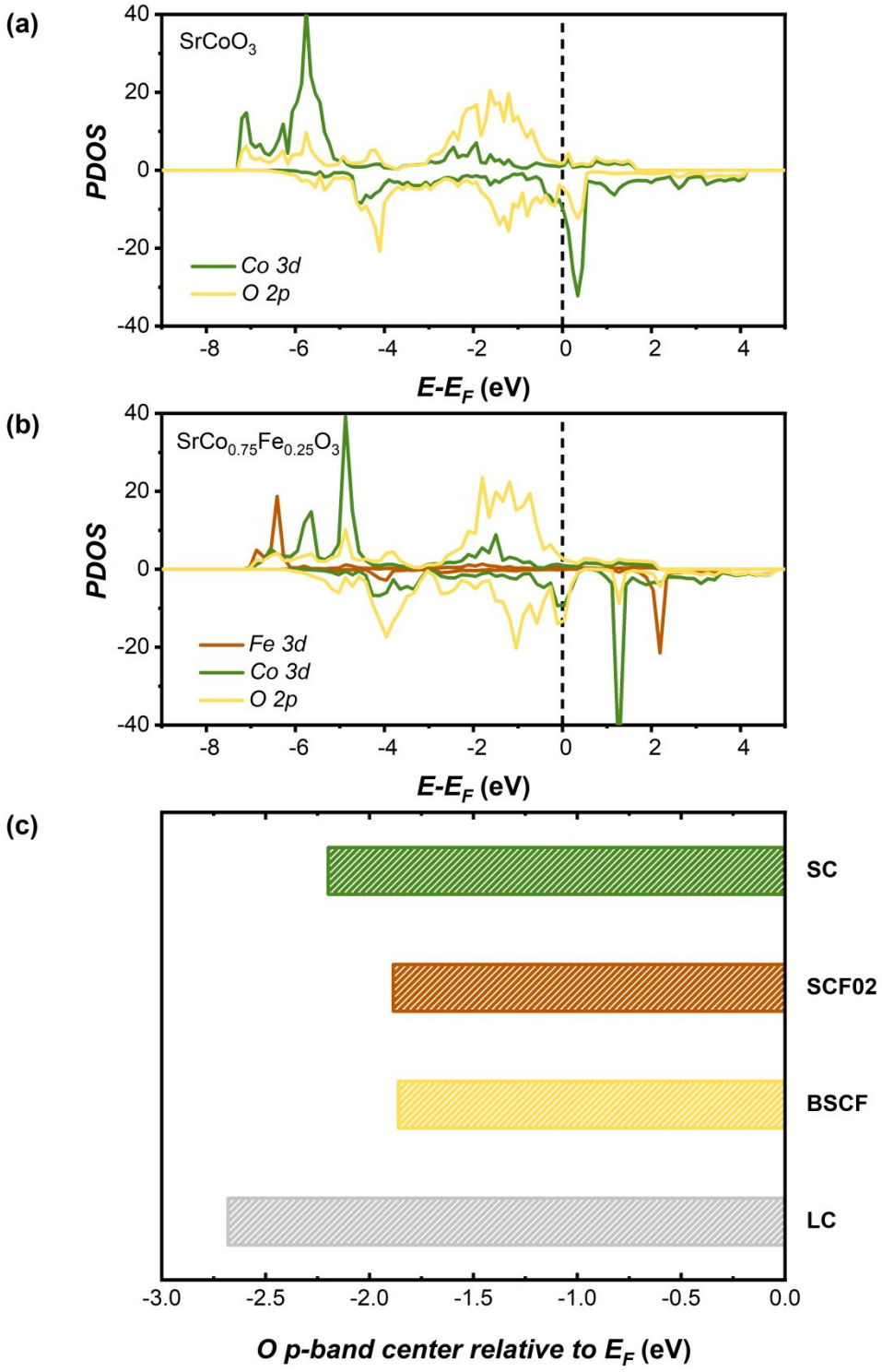

Figure S13. Partial DOS plots of TM 3d-band and O 2p-band for (a) $SrCoO_3$ and (b) $SrCo_{0.75}Fe_{0.25}O_3$. (c) DFT-computed O p-band centers relative to E_F (eV) of $SrCoO_3$ (SC), $SrCo_{0.75}Fe_{0.25}O_3$ (SCF02), $Ba_{0.5}Sr_{0.5}Co_{0.75}Fe_{0.25}O_3$ (BSCF) and $LaCoO_3$ (LC). The close correlation between OER catalytic performance and DFT-computed O p-band center (vs. E_F)

of perovskite oxides was proposed in the literatures.[4,5] The values of O p-band center calculated for SCF02, BSCF and LC are consistent with those reported in the literatures.[4,5]

Table S1. Rietveld refined lattice parameters and reliability factors for SC and SCF02 powders.

Sample	**Structure**	**Space group**	**Lattice parameters a = b = c (Å)**	χ^2	R_p **(%)**	R_{wp} **(%)**
$SrCoO_{3-\delta}$	cubic	$Pm\bar{3}m$	3.8451	1.649	2.09	2.72
$SrCo_{0.8}Fe_{0.2}O_{3-\delta}$	cubic	$Pm\bar{3}m$	3.8570	1.589	1.89	2.49

Table S2. Specific surface area of $SrCo_{1-x}Fe_xO_{3-\delta}$ (x = 0, 0.05, 0.2 and 0.5) measured by Brunauer-Emmet-Teller (BET) analysis.

Samples	**S_{BET} (m^2/g)**
$SrCoO_{3-\delta}$	0.5997
$SrCo_{0.95}Fe_{0.05}O_{3-\delta}$	0.3851
$SrCo_{0.8}Fe_{0.2}O_{3-\delta}$	0.3739
$SrCo_{0.5}Fe_{0.5}O_{3-\delta}$	0.3996

Table S3. Fitting parameters for Sr 3d, Co 2p and O1s XPS spectra of pristine and cycled $SrCoO_{3-\delta}$.

	Pristine SC				**Cycled SC**			
	Sr							
	$3d_{3/2}$	$3d_{5/2}$	$3d_{3/2}$	$3d_{5/2}$	$3d_{3/2}$	$3d_{5/2}$	/	
Binding energy (eV)	135.7	133.7	133.8	132.0	135.2	133.5		
FWHM (eV)	1.61	1.61	1.49	1.49	2.3	2.3		
	Co							
	$2p_{1/2}$	$2p_{3/2}$	$2p_{1/2}$	$2p_{3/2}$	$2p_{1/2}$	$2p_{3/2}$	$2p_{1/2}$	$2p_{3/2}$
Binding energy (eV)	796.6	781.6	795.1	780.0	796.5	781.47	795.06	780.06
FWHM (eV)	3.05	3.05	1.66	1.66	2.6	2.6	1.63	1.63
	O							
Binding energy (eV)	533.1	531.7	529.8		535.7	532.3	529.9	
FWHM (eV)	1.86	1.84	2.05		2.03	2.59	2.13	

Table S4. Fitting parameters for Sr 3d, Co 2p and O1s XPS spectra of pristine and cycled $SrCo_{0.8}Fe_{0.2}O_{3-\delta}$.

	Pristine SCF02				**Cycled SCF02**			
	Sr							
	$3d_{3/2}$	$3d_{5/2}$	$3d_{3/2}$	$3d_{5/2}$	$3d_{3/2}$	$3d_{5/2}$	$3d_{3/2}$	$3d_{5/2}$
Binding energy (eV)	134.8	133.1	133.2	131.4	135.5	133.8	133.0	131.2
FWHM (eV)	1.40	1.40	2.36	2.36	3.44	3.44	0.78	0.78
	Co							
	$2p_{1/2}$	$2p_{3/2}$	$2p_{1/2}$	$2p_{3/2}$	$2p_{1/2}$	$2p_{3/2}$	$2p_{1/2}$	$2p_{3/2}$
Binding energy (eV)	796.7	781.7	795.3	780.3	796.8	781.8	795.1	780.1
FWHM (eV)	3	3	2.05	2.05	3.27	3.27	1.75	1.75
	O							
Binding energy (eV)	/		531.7	529.5	535.6		532.3	529.8
FWHM (eV)			2.29	3.33	2.43		2.80	2.24

Table S5. The concentration of Sr dissolving in the electrolyte during 1-10, 10-50, and 50-100 cycles and the averaged concentration of dissolved Sr per cycle at the three stages.

Samples	Concentration of dissolved Sr (ppb)			Averaged concentration of dissolved Sr per cycle (ppb)		
	1-10 cycles	**10-50 cycles**	**50-100 cycles**	**1-10 cycles**	**10-50 cycles**	**50-100 cycles**
SC	6.77 ± 0.0763	3.24 ± 0.0429	3.63 ± 0.0469	0.677 ± 0.00763	0.081 ± 0.00107	0.0726 ± 9.38E-4
SCF02	7.15 ± 0.104	2.57 ± 0.021	2.21 ± 0.0146	0.715 ± 0.0104	0.06425 ± 5.25E-4	0.0442 ± 2.92E-4

The concentration of trace Sr in the untested 0.1 M KOH electrolyte is 0.776 ± 0.0179.

Table S6. Inductively coupled plasma mass spectrometry analysis of Co and Fe concentrations in the KOH electrolyte after 1-10, 10-50, and 50-100 cycles.

Samples	Co Concentration (ppb)			Fe Concentration (ppb)		
	1-10 cycles	**10-50 cycles**	**50-100 cycles**	**1-10 cycles**	**10-50 cycles**	**50-100 cycles**
SC	0.0169 ± 0.00218	0.0103 ± 0.00272	0.0121 ± 0.0031	0.805 ± 0.113	0.69 ± 0.122	0.695 ± 0.0203
SCF02	0.018 ± 0.00236	0.0139 ± 0.00104	0.0147 ± 0.00611	1.05 ± 0.116	0.965 ± 0.0853	0.872 ± 0.0553

The concentration of trace Co and Fe in the untested 0.1 M KOH electrolyte is 0.0160 ± 0.00145 and 0.748 ± 0.133. Hence, the leaching of B-site cations from SC as well as SCF02 during potential cycling is insignificant.

References

(1) Cornell, R. M.; Schwertmann, U. *The Iron Oxides: Structure, Properties, Reactions, Occurrences and Uses*. John Wiley & Sons, 2003.

(2) Gong, L.; Chng, X. Y. E.; Du, Y.; Xi, S.; Yeo, B. S. Enhanced Catalysis of the Electrochemical Oxygen Evolution Reaction by Iron(III) Ions Adsorbed on Amorphous Cobalt Oxide. *ACS Catal.* **2017,** *8*, 807-814.

(3) Chung, D. Y.; Lopes, P. P.; Farinazzo Bergamo Dias Martins, P.; He, H.; Kawaguchi, T.; Zapol, P.; You, H.; Tripkovic, D.; Strmcnik, D.; Zhu, Y.et al. Dynamic Stability of Active Sites in Hydr(Oxy)Oxides for the Oxygen Evolution Reaction. *Nat. Energy* **2020,** *5*, 222-230.

(4) May, K. J.; Carlton, C. E.; Stoerzinger, K. A.; Risch, M.; Suntivich, J.; Lee, Y.-L.; Grimaud, A.; Shao-Horn, Y. Influence of Oxygen Evolution During Water Oxidation on the Surface of Perovskite Oxide Catalysts. *J. Phys. Chem. Lett.* **2012,** *3*, 3264-3270.

(5) Grimaud, A.; May, K. J.; Carlton, C. E.; Lee, Y. L.; Risch, M.; Hong, W. T.; Zhou, J.; Shao-Horn, Y. Double Perovskites as a Family of Highly Active Catalysts for Oxygen Evolution in Alkaline Solution. *Nat. Commun.* **2013,** *4*, 2439.